ESD-TDR-65-43



# Technical Report 379

# Calibration of a Pressure Sensor for Measurements in Continuum and Rarefied Gas Flows

W. M. Kornegay
J. D. Fridman

8 February 1965

Prepared for the Advanced Research Projects Agency
under Electronic Systems Division Contract AF 19(628)-500 by

Lincoln Laboratory
MASSACHUSETTS INSTITUTE OF TECHNOLOGY
Lexington, Massachusetts

The work reported in this document was performed at Lincoln Laboratory, a center for research operated by Massachusetts Institute of Technology. This research is a part of Project DEFENDER, which is sponsored by the U.S. Advanced Research Projects Agency of the Department of Defense; it is supported by ARPA under Air Force Contract AF 19(628)-500 (ARPA Order 600).

MASSACHUSETTS INSTITUTE OF TECHNOLOGY

LINCOLN LABORATORY

# CALIBRATION OF A PRESSURE SENSOR FOR MEASUREMENTS IN CONTINUUM AND RAREFIED GAS FLOWS

*W. M. KORNEGAY*

*J. D. FRIDMAN*

*Group 35*

TECHNICAL REPORT 379

8 FEBRUARY 1965

LEXINGTON MASSACHUSETTS

ABSTRACT

The free-stream flow behind shock waves produced in the laboratory has been used to obtain a dynamic calibration of a highly sensitive piezoelectric pressure sensor under a wide variety of conditions. Experimental results on the influence of rarefied gas flow on the value of stagnation pressure measured with the sensor are described. This report covers the continuum, slip and transition flow regimes. Design characteristics of the pressure sensor are presented and experimental results are discussed in view of the impact pressure measurements of other authors.

Accepted for the Air Force
Stanley J. Wisniewski
Lt Colonel, USAF
Chief, Lincoln Laboratory Office

## TABLE OF CONTENTS

# CALIBRATION OF A PRESSURE SENSOR FOR MEASUREMENTS IN CONTINUUM AND RAREFIED GAS FLOWS

## I. INTRODUCTION

The measurement of transient pressure phenomena in gases at widely varying gas-flow conditions and regimes has become increasingly important for the study of wind tunnel and shock-tube flows. In particular, such measurements performed in environments simulating high-altitude and high-speed conditions require analysis and interpretation that account for the viscous and rarefied gas effects prevalent at these low pressures. In the experimental investigation of flows having features that cannot be predicted from previous knowledge or theory, it becomes important to use instrumentation that has been properly calibrated in similar flow regimes. The flow regimes in which calibration of the measuring instruments can be performed must have properties (such as the Mach number, the Reynolds number, pressure, density or temperature characteristics) that can be accurately predicted from theory.

Rapidly occurring pressure changes in the flow of gases are best studied in the laboratory using shock waves that are produced in shock tubes. The theory of one-dimensional shock waves is well established, and the techniques by which they are produced and observed are highly developed. Since flow conditions behind the shock wave can be controlled experimentally by setting up the appropriate initial conditions in the shock tube, a wide variety of flow conditions can be simulated.

In order to investigate the structure and mechanics of spherical shock waves at low ambient pressures,[1,2] the response of the pressure sensor instrumentation was measured in similar flow regimes generated in shock tubes. The initial conditions of the spherical shock-wave experiment are such that the extent of flow conditions to which the pressure sensor is exposed range, according to the degree of rarefaction of the gas immediately behind the shock wave, from a continuum to slip and transition flows. It is in these latter flow regimes that, owing to viscous and rarefied gas effects, the pressure distribution along the face of a blunt body will depart from that because of a continuum flow.

A piezoelectric transducer, conventionally used for the measurement of sound pressure, was selected for the spherical shock experiment as a pressure pickup and built as an integral part of a pressure probe. This investigation was conducted to calibrate the sound pressure microphone as a gas flow pressure pickup over the flow regimes of interest. The pressure sensor developed for the present study, its theory of operation, and the experimental and theoretical aspects of the shock-tube calibration will now be discussed.

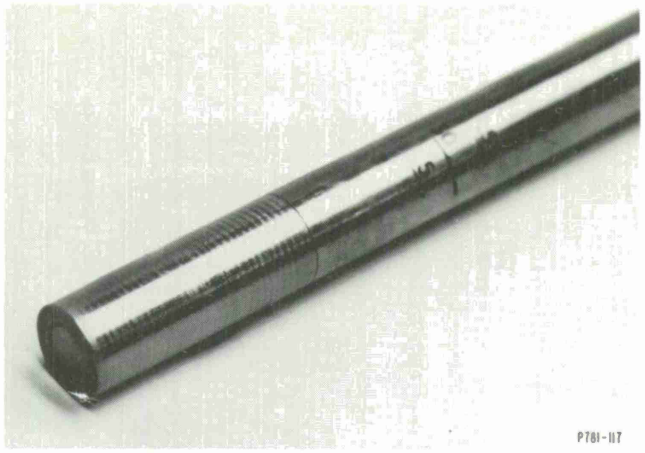


Fig. 1. Pressure sensor probe.

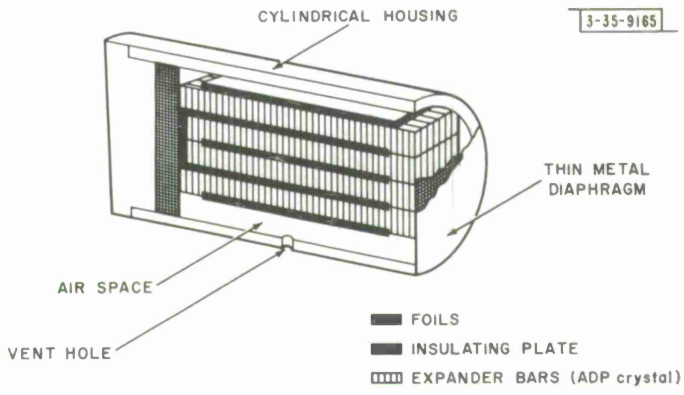


Fig. 2. Internal construction of ADP crystal pressure sensor.

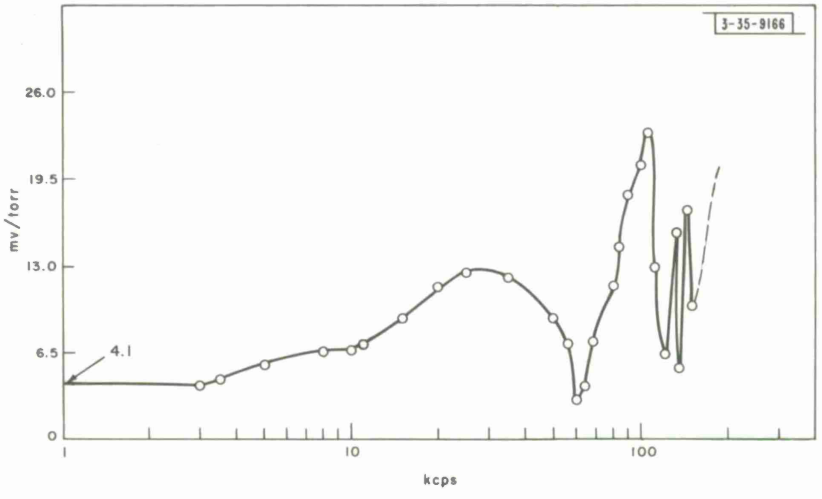


Fig. 3. Frequency response of pressure sensor probe for normal incidence.

## II. PRESSURE SENSOR SYSTEM

The experimental configuration of the shock sphere experiment and the type of spatial measurements that must be made with the pressure sensors have dictated the basic shape and structure of the instrument.

The sensors consist of a piezoelectric crystal mounted at the end of a probe (see Fig. 1) approximately 48 cm in length and 1.25 cm in diameter. The active element of the sensor is composed of four elements of 45° Z-cut ammonium-dihydrogen-phosphate (ADP) crystals. The crystal plates are arranged as expander bars as shown in Fig. 2. Each ADP element has a width of 0.28 cm, a length of 0.476 cm and a thickness of 0.066 cm. The crystal assembly dimensions are, as a result, $0.28 \times 0.476 \times 0.28$ cm. The crystal assembly capacitance $C_K$ is 11 μμf. Any change in pressure acting through a medium in which the sensor is located acts on the end of the bars and compresses them about their undisturbed position. The space around the sides allows for lateral expansion of the bars when they are undergoing longitudinal compression. A hole 0.5 mm in diameter has been provided at the side of the crystal container in order for the ambient gas to reach an equilibrium pressure within the crystal structure. This permits measurement of pressure changes at any low ambient pressure without the need for an otherwise vacuum-tight structure around the crystal.

The crystal assembly is a stiffness-controlled vibrating mechanical assembly which has a resonant frequency of about 140 kcps. This, in turn, is a limit on the frequency response of the transducer. Figure 3 illustrates the frequency-response characteristic of the crystal assembly. For acoustic applications, this characteristic defines the steady-state response of the transducer. A complete discussion of the fundamental requirements for a good standard microphone, together with an analysis of the design which achieves these requirements, may be found in Ref. 3.

The crystal assembly is mounted in a cartridge which connects with one end of a cylindrical probe by means of a miniature two-terminal connector (Fig. 4). An outer housing fits over the crystal assembly housing and screws into the end of the probe near the connector through which the signal leads are brought out from the two electrodes of the crystal. A two-conductor shielded cable is embedded in the probe, one end of which is joined to the mating connector for the signal leads from the crystal and the other end is terminated in a three-pin connector to which the Massa PA-1 preamplifier is connected. The cylindrical probe and three-pin connector are vacuum tight, which permits the complete assembly to be inserted into any low-pressure environment with only the connector to the preamplifier outside the test chamber. The leads coming from the crystal and the crystal housing are electrostatically shielded, protecting the crystal assembly from an extraneous charge due to the presence of a weakly ionized plasma in the test chamber. This shield is brought out through the third connector referred to above. The outer housing is constructed of inconel to provide microwave shielding due to the presence of such a source


Fig. 4. Crystal assembly and probe end.

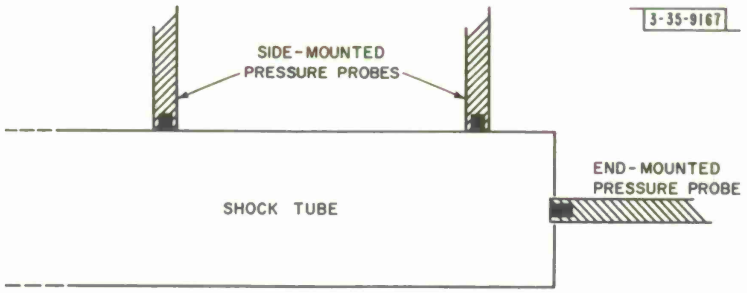


Fig. 5. Arrangement of pressure sensor probes in Harvard College Observatory shock tube.

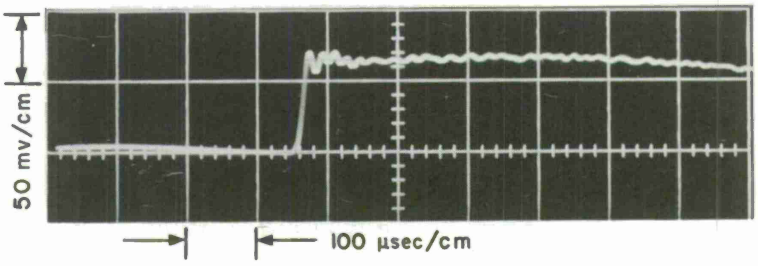


Fig. 6. Pressure transducer response to incident shock wave ($P_1 = 42$ torrs, $M_s = 1.38$) in Harvard College Observatory shock tube.

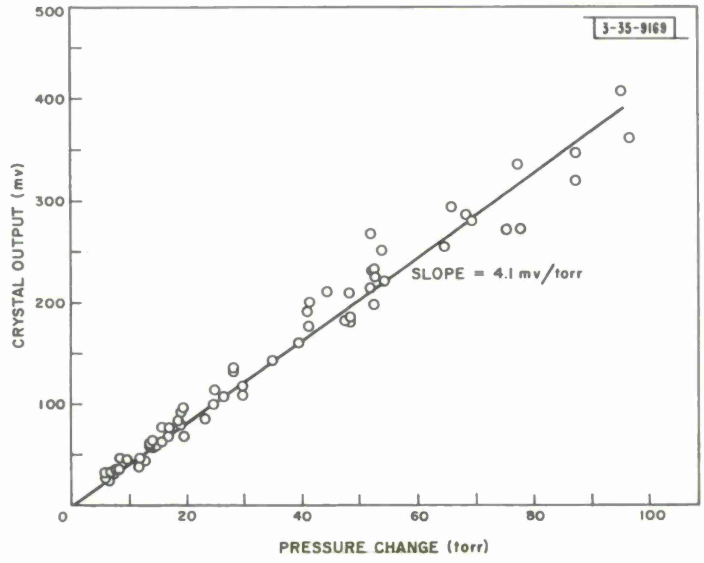


Fig. 7. Voltage response of pressure sensor.

in the test chamber setup. There is no electrical connection between the signal shield and the probe housing; however, they may be connected in the preamplifier to reduce the noise level of the system. The preamplifier and the linear amplifier thus constitute the electronic system with which the response of the crystal assembly to changes in pressure may be properly viewed.

## III. PRESSURE SENSOR CALIBRATION EXPERIMENTS

### A. Calibration Experiments at High Reynolds Numbers

Rapidly occurring pressure changes are associated with shock waves which may be regarded essentially as discontinuous jumps in pressure (see Appendix B). Therefore, one-dimensional shock waves which are produced easily in the laboratory provide an ideal means for making a dynamic calibration of the pressure transducers described above.

A shock tube at the Harvard College Observatory was used to determine the sensitivity of the pressure probes under conditions where the Reynolds number $Re_d$ is large ($Re_d = \rho VD/\mu$, where D is the diameter of the pressure probe, $\rho$ is the density, V is the flow velocity and $\mu$ is the coefficient of viscosity). The shock tube has a circular cross section and is 6.3 cm in diameter. The low-pressure (403 cm long) and high-pressure (90 cm long) chambers are separated by an aluminum diaphragm. These two chambers are closed at the ends remote from the diaphragm and can be evacuated. Shock waves are generated by building up pressure in the high-pressure chamber until the diaphragm ruptures. For the type of diaphragm used, this occurs at about 8 atmospheres. Argon is used as the driver gas. The low-pressure chamber is fitted with openings for mounting pressure probes in the end wall, and also in the side wall at positions 5.1 and 81.3 cm from the end wall as shown in Fig. 5. All probes can be mounted with their sensitive elements flush with the inside wall, thus ensuring minimum interference with the flow. The "end probe" can also be mounted so that it extends down the center of the shock tube from the end plate.

Calibration measurements were made in argon and helium at initial shock-tube pressures from 5 to 60 torrs. We chose 5 torrs as the lower pressure limit because shock-tube performance at low initial pressures is known to be complicated by boundary-layer growth and contact zone phenomena.[4-6]

The pressure gauges in the shock-tube side wall were used to measure the pressure change at the shock front. The Mach number of the incident shock wave was determined from the shock front transit time between the two side-wall pressure gauges. With the initial conditions in the shock tube and the assumption that uniform conditions prevail behind the incident shock wave, the pressure jump $(P_2 - P_1)$ was computed from equations given in Appendix B. A typical oscillogram of the response of a pressure gauge in the side wall, 81.3 cm from the end wall, is shown in Fig. 6. Since the voltage jump ($\Delta V$) of the transducer varies linearly with the applied pressure jump, the slope of a plot of $\Delta V$ vs the theoretical pressure jump $(P_2 - P_1)$ yields the sensitivity of the transducer. The graph resulting from the present calibration experiments is shown in Fig. 7. A least-squares fit of the data yields a gauge sensitivity of 4.1 mv/torr.

To check the internal consistency of these present data, and to determine if the gauge sensitivity for grazing incidence is the same as that at normal incidence, measurements were made using reflected shock waves. Because of the known effects[7] of boundary-layer growth in a shock tube on shock reflection from a closed end tube, the minimum initial pressure used was 10 torrs. At pressures below about 10 torrs, a pressure excess behind the reflected shock was observed.

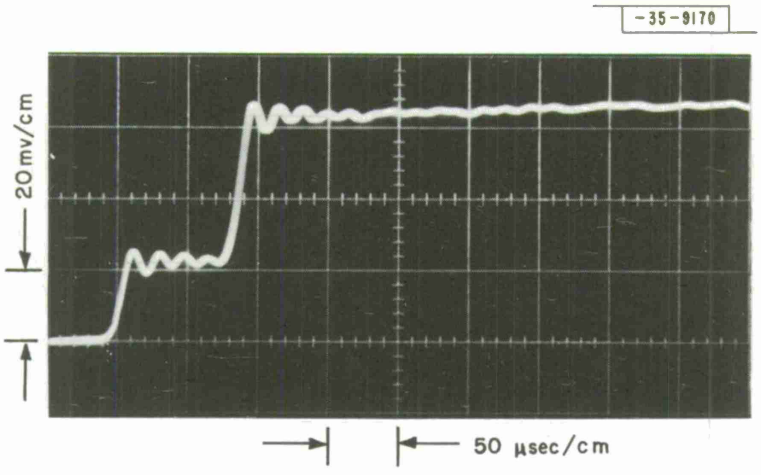


Fig. 8. Response of pressure sensor to incident and reflected shock waves ($P_1$ = 10 torrs, $M_s$ = 1.46) in Harvard College Observatory shock tube.

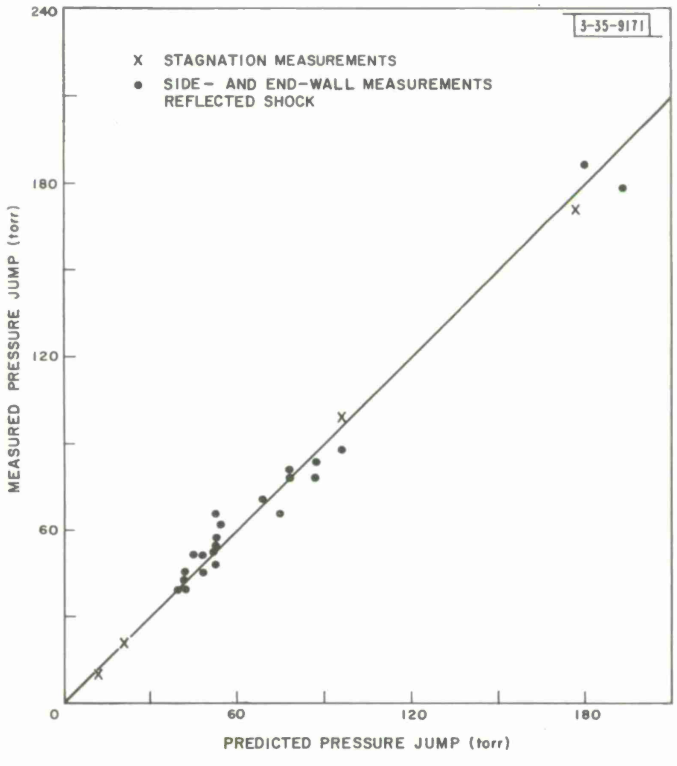


Fig. 9. Pressure sensor measurements vs predictions from ideal theory.

In the reflected shock experiments, gauges were mounted in the end plate of the low-pressure chamber and in the side wall, 5.1 cm from the end. As expected, the gauge in the end wall showed only one pressure jump, and the gauge in the side wall showed two pressure jumps. The double jump can be seen in the oscillogram of Fig. 8. The first voltage jump on the trace is due to the primary shock wave, the second is due to the reflected shock wave. Using the incident shock Mach number, we calculated the state of the gas behind the reflected shock wave in a way analogous to that for the incident shock.

The pressure gauge output-voltage signal was expressed in terms of the corresponding pressure jump ($P_5 - P_1$), using the transducer sensitivity (4.1 mv/torr) determined by the incident shock experiments. If the previous calibration is correct, there should be agreement between the pressure jumps measured and those predicted from the ideal theory. Figure 9 shows that agreement is good; also represented are several measurements of stagnation pressure. To carry out the experiments the gauge was allowed to extend 44 cm in from the end plate. Since the pressure-sensitive element is located at the stagnation point of a blunt body in this arrangement, the pressure jump ($P_t - P_1$) from initial shock-tube pressure $P_1$ to stagnation pressure $P_t$ is measured when the incident shock impinges on the face of the pressure transducer. The theoretical stagnation pressure is obtained from the incident shock Mach number by using the Rayleigh-Pitot formula and the normal shock relations (see Appendix C).

### B. Calibration Experiments at Low Reynolds Numbers

The low-density shock tube at AVCO-Everett Research Laboratory was used to investigate the effect of viscosity on the response of the pressure probes at low Reynolds numbers. This shock tube is 2 feet in diameter and has a low-pressure chamber 60 feet long. In this study one pressure gauge is used at a time, mounted so that the pressure-sensitive element is located at the stagnation point of a blunt body in the flow stream behind normal shock waves (as shown in Fig. 10). The pressure-probe mount (not shown) is inserted through a window in the side of the shock tube and bolted in place by an attached flange. The face of the gauge is approximately 20 feet from the downstream end of the shock tube.

The large cross section of this shock tube eliminates the effect of shock-wave curvature and shock-tube wall boundary layers on pressure measurements. This was not possible with the smaller shock tube at pressures below a few torrs. In this large-diameter shock tube, it should be possible to attribute any deviations from pressures predicted by the Rayleigh-Pitot formula in the continuum regime to viscous effects and rarefied gas phenomena.

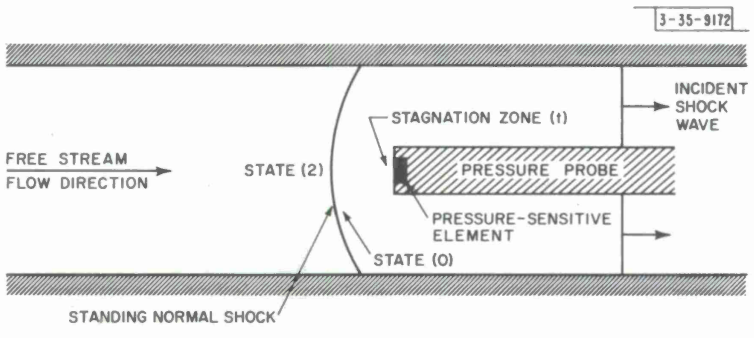


Fig. 10. Blunt probe in supersonic free-stream flow.

Measurements were made in argon at initial shock-tube pressures ranging from 0.020 to 1.0 torr. An explosive mixture of oxygen and hydrogen diluted with nitrogen was used as a driver gas. Mach numbers of the incident shock waves ranged from 8.8 to 10.8, while the flow Mach number (of the gas immediately behind the shock front) was 1.31 ± 0.01. Heat transfer gauges were used to monitor the speed of the shock wave along the length of the shock tube. It was not possible to detect shocks weaker than about Mach 9 in argon because of the limited sensitivity of the heat-transfer gauges used.

In a shock tube, temperature changes invariably accompany pressure changes. At Mach 10 the free-stream translational temperature is about 10,000 °K in argon, and the stagnation temperature is even higher. Because of heat transfer, the ADP crystal response to temperature is always delayed with respect to pressure response. In order to increase this delay, the active face of the transducer was covered with a thin layer of vacuum grease. Inspection of the probe face after several experiments did not reveal any evidence of excessive heating. Also no adverse effects which could be attributed to heating of the ADP crystal were observed on the pressure traces.

Observation time for reliable data was limited to about 100 μsec. The possibility of waves reflected from the pressure gauge mount interacting with the standing shock and the flow in the vicinity of the pressure gauge imposed this limitation. Because of short observation times and known thermal ionization rates for argon,[8,9] it is reasonable to assume that the effect of ionization on the impact pressure was negligible in these experiments. If air is used, one cannot make this "frozen flow" assumption. Activation of the inactive degrees of freedom, such as vibration and dissociation, at high temperatures would make it necessary to follow the chemical relaxation in the free-stream and stagnation zones in order to interpret pressure measurements.

For each experiment the shock-wave Mach number, which was computed from the measured shock speed, was used to predict the theoretical pressure of the gas in the stagnation zone. It was assumed that the ideal shock-tube theory and the Rayleigh-Pitot formula for continuum flow are valid under prevailing experimental conditions. The Reynolds and flow Mach numbers of the gas behind the normal shock wave were also calculated from ideal theory. Viscosities were taken from a paper by Amdur and Mason.[10] Measured stagnation (impact) pressure was inferred from the pressure gauge measurements using a sensitivity of 4.1 mv/torr. A common method

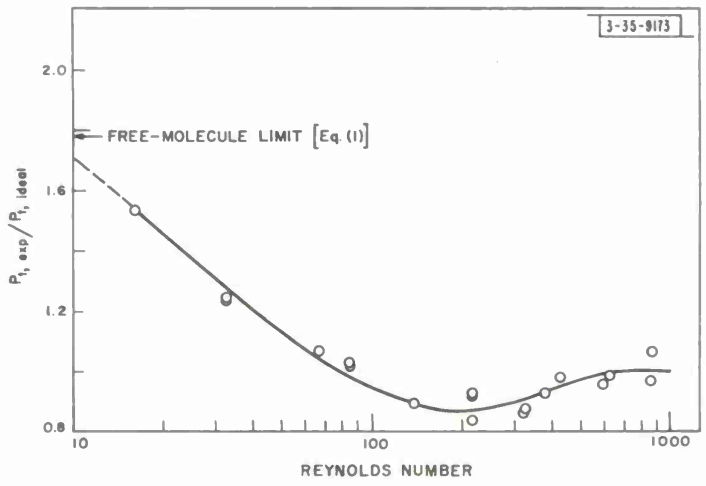


Fig. 11. $(P_{t,exp}/P_{t,ideal})$ vs Reynolds number.

of presenting the viscous correction data[11] is to divide the experimentally determined impact pressure by the ideal impact pressure, and to plot these as a function of Reynolds number. Data presented in this manner are shown in Fig. 11.

## IV. DISCUSSION

The dynamic response of an instrument is a measure of its capability to reproduce accurately signals with well-defined frequency and amplitude characteristics. This response is represented by the change in amplitude and phase occurring as a result of the response of the measurement system to a succession of frequency-dependent forcing functions. This relationship in the frequency domain may be expressed correspondingly in the time domain by a function representing the response of the system to a time-dependent forcing function. The time-function representation is usually particularized in the form of an aperiodic function such as a step or ramp function. In the case of the pressure sensor, the experimental determination of the dynamic response has been obtained from recorded pressure vs time responses to a pressure step function produced in shock tubes. However, in the case of the sound microphone, such a characteristic is obtained experimentally by a sinusoidal forcing function over a wide range of frequencies. The entire amplitude-phase vs frequency relationship over the required frequency spectrum is related to the single response due to a time function by means of the Fourier transform by well-known relationships.[12]

Let us now compare results obtained for the pressure sensor by the frequency and time. The time response shown in Fig. 12(a), obtained on the AVCO shock tube, and the amplitude-vs-frequency characteristic of the pressure sensor shown in Fig. 3 are, in fact, related.[12] The ringing that has invariably been observed on every normal shock recording corresponds to a frequency of about 100 kcps. Cause of this ringing is the excitation of resonant modes of vibration within the piezoelectric crystal and its structure. The acoustic calibration of the pressure sensor indicates that at about this frequency the pressure sensor amplitude peaks and keeps on oscillating to a frequency of 150 kcps. Sensitivity of the pressure sensor at 4.1 mv/torr corresponds to the average jump in voltage. One observes that this level of sensitivity corresponds to the flat portion of the amplitude-vs-frequency characteristic for normal and/or grazing incidence. The average level of the recorded signal and ringing of the pressure sensor is schematically shown in Fig. 12(b) for a typical case of normal shock-wave impact.

The high-frequency limit of the amplitude-vs-frequency characteristic is an approximate measure of the rise time of an instrument, which is usually defined as the time required for the response to go from 10 to 90 percent of its final value. It can be estimated approximately by the formula

$$T_r = \frac{K}{B}$$

where

$T_r$ = rise time in seconds

K = 0.30 to 0.35 for small signal overshoots

B = bandwidth of transducer in cps.

Bandwidth, for the case of the pressure sensor, may be defined as the frequency range over which the response does not change by more than 3 db beyond the flat portion of the amplitude-vs-frequency characteristic. For the pressure sensor the bandwidth for grazing incidence is about

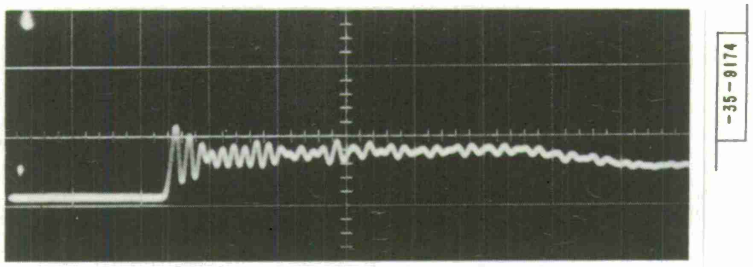


Fig. 12(a). Stagnation pressure measurement in argon ($M_s = 8.8$, $P_1 = 0.35$ torr) in AVCO-Everett shock tube.

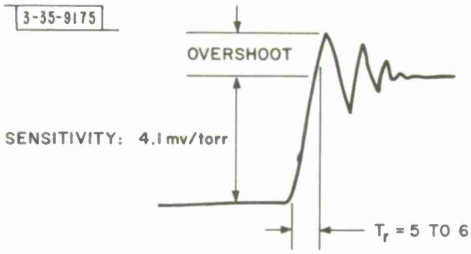


Fig. 12(b). Typical pressure sensor response for normal incidence of a plane shock wave.

80 kcps, which therefore limits the rise time to about 4 μsec. Rise times obtained from shock measurements indicate that it is between 5 and 6 μsec.

The relationship obtained between the voltage output and change in pressure or, in other words, the measured sensitivity of the transducer is linear with pressure and proportional to the change in pressure. This is expected as a result of the equation $V_K = S_{ji}$ (transducer constant) derived in Appendix A. Therefore, the transducer constant is linear with pressure over a wide range. This is clearly a distinctive characteristic of piezoelectricity.[13]

The conversion constant of 4.1 mv/torr was derived by recording the voltage change at the shock front measured by pressure sensors at grazing incidence to the propagating shock wave, and by computing the expected pressure change from the measured shock Mach number. A sufficient demonstration of the accuracy of this technique is that the check on the internal consistency of this measurement results in an agreement as good as that shown in Fig. 9.

Under ordinary conditions, the Rayleigh formula for supersonic flow and the isentropic relation for subsonic flow may be used to calculate the stagnation pressure, provided the flow Mach number and free-stream pressure are available. At low pressures, where the Reynolds number based on the impact probe diameter is small, the measured stagnation pressure usually departs radically from theoretical values. This phenomenon occurs because the terms involving the viscosity in the Navier-Stokes equation cannot be neglected in solving the stagnation streamline flow in the vicinity of the probe head, and because the occurrence of slip flow causes the zero-velocity boundary condition at the surface of the probe to become invalid.

A rather thorough investigation of impact pressure probes at low pressures in supersonic and subsonic air streams has been carried out by Sherman[11] at the University of California and by Enkenhus[14] at the University of Toronto. Kosterin, et al.,[15] have also studied the functional dependence of impact pressure on Reynolds and Mach numbers. Sherman found that impact pressure probe measurements could be interpreted by the rather simple fluid theory as long as

the Reynolds number $Re_d$ based on probe diameter is greater than about 200. When the Reynolds number is less than 200, the measured impact pressure is a function of the Reynolds number, Mach number and probe shape.

The data presented in Refs. 11, 14 and 15 provide correction factors for viscous effects on measured impact pressure for probes of various shapes. Since the true flow Mach and Reynolds numbers are not known initially in most experiments, one must use an iterative procedure in applying these viscous correction factors. For blunt-nosed probe corrections, however, there is some doubt[16] whether we can use (even as a guide) corrections evolved[11,14,15] for hydrodynamically shaped probes. Existing theories are inadequate to predict the functional dependence or impact pressure on Reynolds and Mach numbers for blunt-nosed pressure probes at low Reynolds numbers.

The characteristic shown in Fig. 11 is that of the blunt-nosed pressure sensors used in our experiments in viscous and rarefied gas-flow regimes. For high Reynolds numbers, above 600, there is no departure of the experimentally measured stagnation pressure from that theoretically calculated by use of the Rayleigh-Pitot formula. Thus, this segment of the curve is clearly in the continuum regime where all classical relationships still hold. Below a Reynolds number of 600 and down to a minimum at about 200, there is a dip in the curve wherein the actual stagnation pressure at the sensor departs from that predicted by the Rayleigh-Pitot formula – this is the onset of slip flow. An increase of the influence of viscosity on the flow in the neighborhood of the surface of the blunt body causes a decrease of the impact pressure close to the stagnation point.[17] It has been shown by Kosterin, et al.,[15] that the appearance of the dip is independent of the probe diameter or the thickness of the boundary layer about the blunt body; thus it is dependent only on the slip-flow condition. A further decrease in pressure beyond the dip from 0.175 to about 0.100 torr (corresponding to a Reynolds number in the 200 to 80 range) results in an increase in rarefaction accompanied by a decrease of the irreversible loss during passage of the shock front; that is, the shock-layer growth and pressure jump across the shock become smaller, resulting in an increase of pressure at the stagnation point. At a Reynolds number of about 80, the measured stagnation pressure is equal to that corresponding to a continuum flow. At still lower Reynolds numbers, the measured value rises well above the value predicted by ideal theory. This occurs at about the onset of transitional flow, resulting in a stagnation pressure ratio that is well above unity.

Potter and Bailey[17] investigated the same phenomena in a low-density, supersonic wind tunnel using orifice-type blunt and hemispherical probes. They found relationships for their particular probes in a low Reynolds number, supersonic flow of argon very similar to that of Fig. 11. There is a qualitative relationship between the behavior of the stagnation pressure and Probstein and Kemp's regime[18] of rarefied flow. Thus, the decreasing trend of $P_{t,\,exp}/P_{t,\,ideal}$ at intermediate Reynolds numbers seems to be related to viscous-layer phenomena, whereas the reversal to an increasing trend seems to be related to merged-layer phenomena.

For very small Reynolds numbers, the characteristic of Fig. 12 can be projected beyond the actual measurements to a free-molecule limit derived by Enkenhus.[14] It can be shown that for an orifice probe in a free-molecular flow

$$\frac{P_{t,\,exp}}{P_{t,\,ideal}} = \left[\left(1 + \frac{\gamma - 1}{\gamma} S^2\right)^{1/2} \cdot \left\{e^{-S^2} + S\sqrt{\pi}\,[1 + \mathrm{erf}(S)]\right\}\right] \frac{P_2}{P_{t,\,ideal}} \quad , \tag{1}$$

where S (molecular speed ratio) is related to the flow Mach number by $S = \sqrt{\gamma/2}\, M_2$. The distinguishing characteristic of the orifice probe is that it permits the passage of individual gas molecules into the gauge volume, without hindering their collection. However, in the free-molecule regime all types of probe structures used are identical because we assume that (a) the mean free path is so large that intermolecular collisions may be neglected outside the probe, (b) molecules striking the walls are diffusely reflected, and (c) outgassing from the interior of the pressure sensor is absent. Thus we can apply Eq. (1) with confidence to derive the free-molecule limit expected for the piezoelectric pressure sensors. The result of the computation is shown in Fig. 11.

## V. CONCLUSIONS

Results of the investigation show that the stagnation pressure at the blunt face of a pressure sensor probe is dependent on the flow phenomena that occur in the continuum, slip, transition, and free-molecular regions of the flow regime. The calibration characteristic for continuum-flow conditions precisely satisfies the Rankine-Hugoniot and Rayleigh-Pitot relations; for the other flow regimes, it is dependent on viscous and rarefied gas effects.

As a result of limitations imposed by the shock-tube experimental facility, this study has been confined to a narrow variation in flow Mach number. There is good indication in the work of Kosterin, et al.,[15] that the dependence of the impact pressure upon Mach as well as Reynolds numbers is important. Therefore, it should be pointed out that the calibration we have performed of the pressure sensor at low Reynolds numbers is limited to flows in argon with a flow Mach number of $1.31 \pm 0.01$. However, by the same token, this calibration will be valid for all such flows having a $Re_d/M$ ratio ranging from 765 to 6.1 and presumably lower.

The pressure probe, however, can be used without limitation in any continuum flow. The conversion constant of 4.1 mv/torr measured at the end of the probe corresponds, in reality, to a crystal sensitivity of 16.8 mv/torr. To the best of our knowledge, literature on piezoelectric pressure transducers[12,19] does not report a sensor with such outstanding sensitivity. However, this sensitivity has been obtained at the cost of a relatively slow time response of 5 to 6 μsec. Thus, in the design of the ADP crystal head, sensitivity was traded off for response time by use of thicker crystal slabs.

## APPENDIX A
## THEORY OF PIEZOELECTRIC FORCE PICKUP

A piezoelectric element[20] is a natural or artificially polarized crystal that produces, within certain limits, a charge proportional to an applied force. The charge is accumulated in the direction of polarization of the crystal. Two electrodes are attached to the planes of polarization of the crystal, permitting the charge produced by the piezoelectric action to be recorded by proper instrumentation.

A piezoelectric force pickup consists of one or more piezoelectric elements stacked in a suitable manner, supported by a rigid base and mounted in an enclosure. Signal output by the pickup can then be amplified and displayed electronically. The plane of cutting, the mode of polarization and the force applied on the piezoelectric elements determine their suitability for application to the measurement of normal forces, shear forces, tension, bending, and combinations thereof.

Let $F_D$ be the total external force on the diaphragm of the pickup, and let $F$ be the force transmitted to each element on the n-element crystal array. Then the stress $S_{yz}$ in the direction of the x-axis, acting on the surface $A_{yz}$ perpendicular to the x-axis, is

$$S_{yz} = \frac{F_x}{A_{yz}} \text{ dynes/cm}^2 \quad .$$

In the absence of an electric field, polarization field $P$ is produced by a second-order tensor stress system

$$P_k = d_{ke} J_e \qquad (k = 1, 2, 3;\ e = 1, 2, 3, 4, 5, 6) \quad ,$$

where

$$J_1 = SX_x,\ J_2 = SY_y,\ J_3 = SZ_z,\ J_4 = SY_z,\ J_5 = SX_z,\ J_6 = SX_y$$

and

SX, SY, SZ = components of stress S (dynes/cm$^2$)

x, y, z = crystal coordinate axis

$d_{ke}$ = piezoelectric charge (statcoulombs/dyne)

P = polarization (statcoulombs/cm$^2$)

$J_e$ = tensor components of stress system.

The six components of the stress system are due to compressions along the three crystal coordinate axes and shearing stresses with respect to the three planes normal to the axes.

On the two opposite surfaces of polarization, the surface charge density is equal to the polarization $g_k = P_k$, where $g_k$ = charge density (statcoulombs/cm$^2$). Hence the total charge

$$Q_k = g_k A_k = d_{ke} \cdot J_e A_k \quad .$$

The total charge per piezoelectric element is

$$Q'_k = \frac{Q_k}{n} \quad ,$$

where

$n$ = number of elements in piezoelectric pickup

$Q_k$ = total charge deposited per piezoelectric element.

The potential across the two surfaces of the crystal element is given by

$$V'_k = \frac{Q'_k}{C'_k} \quad ,$$

$$C'_k = \frac{KA_k}{4\pi t'} \text{ (capacitance per element in } \mu\mu f) \quad , \tag{A-1}$$

where

$K$ = dielectric constant

$t'$ = thickness per element (cm).

If all elements are connected in parallel (see Fig. 1)

$$C = nC'_k \quad . \tag{A-2}$$

Therefore, capacitance of pickup C ($\mu\mu f$) is

$$C = nC'_k + C_o$$

where

$C_o$ = external shunt leakage capacitance due to leads, wires, etc.

Hence, the over-all voltage developed across the transducer will be

$$V_k = \frac{nQ'_k}{nC'_k + C_o} = \frac{nd_{ke}J_eA_k}{(nKA_k/4\pi t') + C_o} \quad . \tag{A-3}$$

If $C_o \ll C'_k$, then

$$V_k = \frac{d_{ke}J_e}{K/4\pi t'} = (g_k t') \cdot \text{constant} \quad ,$$

or

$$V_k = \left(\frac{F_j}{A_i} d_{ke} t'\right) \cdot \text{constant} \quad (j = x, y, z;\ i = xy, yz, xz) \quad , \tag{A-4}$$

that is,

$$V_k = F_j \cdot K' \quad , \tag{A-5}$$

or

$$V_k = S_{ji} \cdot K \quad , \tag{A-6}$$

where

$K'$ = transducer constant

$K = K'/A_i$.

The charge produced at the electrodes of the piezoelectric transducer is therefore a voltage proportional to the applied force. A faithful reproduction of the signal with minimum leakage requires a circuit time constant RC, where $C = nC_k' + C_o$ and R is the external circuit resistance. In fact, by Eq. (A-3), the transducer capacitance $nC_k'$ and the external capacitance $C_o$ can be selected to yield a value for the over-all voltage $V_k$ developed across the transducer (the smaller the total capacitance C, the larger the $V_k$). The value of $C_o$ can be adjusted in the external circuit; however, $C_k'$ is dependent on the basic configuration of the transducer element. The built-in value of $C_k'$, which is proportional to the number of elements in the transducer and inversely proportional to the thickness per element, is the basic factor that determines the transducer sensitivity. A small value of $C_k'$ implies that, for a given available crystal container volume, the number of elements per stack will be small, even unity, and by Eq. (A-1) that the thickness per element will be large. Thus a high voltage sensitivity may be obtained. On the other hand, making $C_k'$ small will yield a correspondingly low time constant and this will result in transducer insensitivity to very fast pressure changes. As a result the rise time of the pickup will suffer. Hence, for a fast transducer rise time a large value of $C_k'$ is desired. There exists, therefore, a trade-off between voltage sensitivity and rise time that is solely dependent on the number of elements per stack and the thickness per element.

A figure of merit proportional to the quantity $Q = CV$ may be taken as a measure of the performance of the particular piezoelectric crystal arrangement. Thus the figure of merit expresses the relationship between voltage sensitivity and rise time in form of a convenient design parameter that can be used for comparing the performance of piezoelectric transducers.

The effect of stacking the piezoelectric pickup in parallel by a number of elements has the following effects on the transducer characteristics:

(1) Capacitance proportional to n
(2) Total charge $Q_k$ proportional to n
(3) Constant voltage independent of n.

Voltage sensitivity of the transducer is proportional to the thickness per element which, in turn, determines the response time of the crystal array. A high figure of merit is obtained by stacking piezoelectric elements in parallel. The manufacturing problem of cutting very thin slices of the piezoelectric crystal in its proper orientation, together with the sensitivity desired at the transducer output, determine the number of elements to be used in any given transducer enclosure. The lower limit on the response time of the transducer is determined by the natural frequency of vibration of the crystal and the mechanical enclosure of which it is a part.

## APPENDIX B
## SHOCK WAVES IN GASES

### I. SHOCK WAVES

In its simplest form, the shock wave is regarded as a thin front of the order of a few molecular mean free paths thick. The front is characterized by an abrupt, almost discontinuous, increase in the pressure, temperature, density and velocity of the gas into which it propagates. The Mach number $M_s$ of the shock wave is a convenient measure of its strength. Shock strength is controlled by the starting pressure and temperature ratios.

Formation of a shock wave may be visualized by realizing that a series of compressional waves which propagate into the low-pressure gas is set up when the driver gas expands into the low-pressure gas of a shock tube. Compressional waves are of finite amplitude and will raise the temperature of the low-pressure gas by adiabatic compression. These small pressure disturbances will propagate into the gas with the speed of sound. This means that each successive wave will eventually overtake and coalesce with the preceding waves, with the resultant formation of a shock wave.

### II. SHOCK TUBE

The behavior of shock waves is most conveniently studied by using a shock tube. A shock tube consists essentially of two sections of long pipe of uniform cross section, a chamber and a channel, separated by a thin diaphragm and closed at the downstream and upstream ends. The diaphragm may be metal, celluloid, cellophane, or some similar material, depending on the pressure difference it is to withstand. At the time the diaphragm is removed, the chamber containing the driver gas is at high pressure. The channel contains gas (at a lower pressure) through which the compressions that rapidly become a shock wave are propagated. The high-pressure region may be built up mechanically behind the diaphragm, or it may be induced by such means as chemical explosion, electrical discharge or exploding wires.

The history of the ideal shock-tube flow is shown schematically in Fig. B-1. The X-t diagram shows the space time loci of the waves at a time t after the shock is initiated. Following removal of the diaphragm (X = 0, t = 0), the wave system consists of:

(a) A plane shock wave (incident shock wave) moving to the right, adiabatically compressing the channel gas [region (1)] and setting it into motion.

(b) A contact surface following the shock wave into the channel. (Ideally, the contact front is represented as a discontinuity in temperature, density, entropy and internal energy; i.e., it is a surface separating two thermodynamically different states that are moving at the same flow velocity and pressure.)

(c) A centered rarefaction wave, the head of which moves to the left into the high-pressure region (4) at the local sonic velocity, isentropically expanding the chamber gas and setting it into motion at the same velocity and pressure existing behind the shock wave.

When the incident shock wave reaches the closed end of the low-pressure section of the shock tube, it is reflected into the region (2) originally behind the incident shock wave. Gas in this region is brought to rest and further heated and compressed.

The wave system in a shock tube can be a much more complicated picture than that presented here. Waves initially produced can undergo many interactions, depending on the length of the shock tube used and the relative lengths of the channel and chamber.[21]

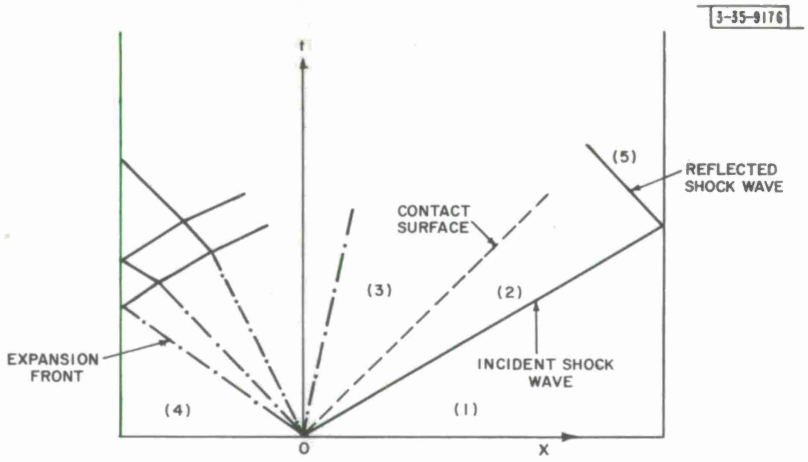


Fig. B-1. X-t diagram showing progress of shock and expansion waves following diaphragm burst.

## III. BASIC EQUATIONS FOR SHOCK WAVES

Rather complete details of the theory of shock waves and a full description of the assumptions inherent in the development of the ideal, one-dimensional, unsteady flow in a shock tube may be found in the literature.[22,23] Thus, in this section we will present only the basic shock relations that pertain to the experimental results presented in Sec. III. Interested readers may find the derivation of these relations in the references cited.

The relationship between the region of undisturbed gas in front of the shock wave and the region of uniform gas in statistical equilibrium behind the shock wave is uniquely determined by the Rankine-Hugoniot or basic shock relations. Denoting pressure, density, temperature, sound speed and Mach number by P, $\rho$, T, a, and M respectively, and using the subscripts 1 and 2 to identify the regions to the front and back of the shock wave respectively, we have the following formulas for a perfect gas:

$$\frac{P_2}{P_1} = \frac{2\gamma_1 M_s^2 - (\gamma_1 - 1)}{\gamma_1 + 1} \quad , \tag{B-1}$$

$$\frac{\rho_2}{\rho_1} = \frac{(\gamma_1 + 1)\, M_s^2}{(\gamma_1 - 1)\, M_s^2 + 2} \quad , \tag{B-2}$$

$$\frac{T_2}{T_1} = \frac{[2\gamma_1 M_s^2 - (\gamma_1 - 1)]\,[(\gamma_1 - 1)\, M_s^2 + 2]}{(\gamma_1 + 1)^2\, M_s^2} \quad , \tag{B-3}$$

$$M_2 = \frac{2(M_s^2 + 1)}{[2\gamma_1 M_s^2 - (\gamma_1 - 1)]^{1/2}\,[(\gamma_1 - 1)\, M_s^2 + 2]^{1/2}} \quad , \tag{B-4}$$

where $M_s$ is the Mach number of the incident shock wave. Note that if the initial conditions (quantities with subscript 1) are known and if the shock Mach number $M_s$ is determined, all other flow quantities may be calculated. Velocity $U_s$ of the shock front is determined by measuring the time between its arrival at two stations along the shock-tube wall, which are a known

distance apart. When this velocity is divided by the speed of sound, $a_1 = \sqrt{\gamma_1 R T_1 / m_1}$, one obtains the shock Mach number. R is the universal gas constant, and $\gamma$, T and m are the specific heat ratio, temperature and molecular weight, respectively, of the gas into which the shock propagates.

The variation of pressure, density and temperature across the reflected shock wave is given by the following relations:

$$\frac{P_5}{P_2} = \frac{\alpha_1 + 2 - P_{12}}{1 - \alpha_1 P_{12}} \quad , \tag{B-5}$$

$$\frac{\rho_5}{\rho_2} = \frac{1 + \alpha_1 P_{52}}{\alpha_1 + P_{52}} \quad , \tag{B-6}$$

$$\frac{T_5}{T_2} = \frac{P_{52}(\alpha_1 + P_{52})}{1 + \alpha_1 P_{52}} \quad , \tag{B-7}$$

where $\alpha = (\gamma + 1)/(\gamma - 1)$ and $P_{ij} = P_i/P_j$.

In these relations, the subscript 5 denotes the region behind the reflected shock wave (other subscripts have the same meaning assigned earlier in this section).

It should be remembered that, in the derivation of the above shock relations, the specific heat ratio $\gamma$ is assumed constant. Hence at high temperatures where the gas is vibrationally or electronically excited, dissociated, or ionized appreciably, these equations are not accurate. When these "inactive" degrees of freedom are excited, temperature, density and pressure across the shock front can be calculated from the Rankine-Hugoniot equations according to a method first developed by Bethe and Teller.[24] This method of treating imperfect gas effects, along with several other methods, is described in detail in Ref. 23.

The shock Mach number, which is the basic parameter in Eqs. (B-1) through (B-7), is a measure of the shock strength. It is related to the pressure ratio $P_{41}$ across the diaphragm by

$$P_{41} = \left( \frac{2\gamma_1 M_s^2}{\gamma_1 + 1} - \frac{\gamma_1 - 1}{\gamma_1 + 1} \right) \left[ 1 - \frac{\gamma_4 - 1}{\gamma_1 + 1} \frac{(M_s^2 - 1)}{M_s (a_4/a_1)} \right]^{-(2\gamma_4/\gamma_4 - 1)} \quad , \tag{B-8}$$

where $a_4$ is the sound speed of the driver (high-pressure) gas and $a_1$ is the sound speed of the low-pressure gas. The assumptions which enter Eq. (B-8) are: (a) constant heat capacity, (b) perfect diaphragm burst, and (c) one-dimensional flow without viscosity or heat transfer. Since one or more of these assumptions break down at most pressure ratios, there is usually a discrepancy between Eq. (B-8) and experiment. However, the equation serves as a useful guide in setting up experiments.

From Eq. (B-8) it will be noted that the two important parameters governing shock strength are the diaphragm pressure ratio $P_{41}$ and the diaphragm sound-speed ratio $a_4/a_1$. In practice, little effect can be achieved through the specific heat ratios. The limiting value of $M_s$ attained asymptotically, as $P_{41}$ goes to infinity and $a_4/a_1$ remains finite, is

$$\lim_{P_{41} \to \infty} M_s = \frac{\gamma_1 + 1}{2(\gamma_4 - 1)} \frac{a_4}{a_1} \sqrt{\left[ \frac{\gamma_1 + 1}{2(\gamma_4 - 1)} \frac{a_4}{a_1} \right]^2 + 1} \quad .$$

This indicates a need for large $a_4/a_1$ and low $\gamma_4$ to obtain strong shock waves. Since $a^2 = \gamma RT/m$, it is possible to obtain a large $a_4/a_1$ by choosing a low molecular-weight gas for the driver [region (4)] and a high molecular-weight gas for the driven gas [region (1)]. On the other hand, one could preheat the gas in the drive, making $T_4 > T_1$. Hall[25] gives an excellent review of this subject.

## APPENDIX C
## SUPERSONIC AND SUBSONIC FLOW ABOUT A SPHERE

### I. DETACHED SHOCKS

When an axially symmetric body (hereafter called a probe) with a flat nose is placed in a uniform supersonic stream parallel to the flow direction, a curved shock wave stands ahead of the body.[26] This is shown schematically in Fig. 11. If the probe does not have a blunt nose, but is a very slender body or a wedge of sufficiently small half angle, the shock wave will be attached. The detached shock wave, which is generated when the supersonic flow impinges on the blunt body, becomes stationary because the mass of the gas in which it propagates travels at a speed equal, but in opposite direction, to that of the shock wave. Note that a detached shock wave is also produced by the movement of a blunt object through a gas at velocities in excess of the sound velocity.

The time required for the detached shock to form and its detachment distance depend on the flow Mach number $M_2$ and the geometry of the body. Reference 27 reports on a thorough investigation of this problem for wedges. The available data for axially symmetric blunt-nosed bodies are summarized in Fig. 4-15 of Ref. 22.

### II. STAGNATION ZONE AND FORMULAS

If we consider the supersonic stream as being the flow behind the normal shock wave discussed in Appendix B, then the free stream pressure $P_2$ and flow Mach number $M_2$ can be readily determined by measuring the speed of the shock. On the other hand, the Mach number of the flow ahead of the detached shock wave may be found by measuring the pressure on the blunt end of the probe. The assumptions one makes in carrying out the measurement are:

(a) At the point where the stagnation streamline crosses the standing shock wave, it is normal to the shock wave. This criterion is satisfied by placing the probe axis parallel to the flow direction.

(b) After the particles pass through the standing shock wave, they are decelerated isentropically to zero velocity in the region between the shock wave and the blunt body. This region of gas at zero velocity ahead of the blunt body is called the stagnation zone.

The fact that the stagnation streamline crosses the shock wave normal to it means that the pressure across the standing shock front can be related by the simple shock relations given in Sec. III of Appendix B,

$$\frac{P_o}{P_2} = \frac{2\gamma M_2^2 - (\gamma - 1)}{\gamma + 1} \quad . \tag{C-1}$$

This means that gas entering through the stagnation streamline will pass through a normal shock and will thus decelerate (becoming subsonic). Adiabatic isentropic compression of the gas at state (0) (see Fig. 10) along the stagnation streamline to zone (t) is represented by the well-known adiabatic isentropic relation

$$\frac{P_t}{P_o} = (1 + \frac{\gamma - 1}{2} M_2^2)^{\gamma/\gamma-1} \quad . \tag{C-2}$$

The Mach number of the subsonic gas in state (0) is related to that in state (2) by

$$M_o^2 = \frac{1 + \frac{\gamma - 1}{2} M_2^2}{\gamma M_2^2 - \frac{\gamma - 1}{2}} \quad . \tag{C-3}$$

We write

$$\frac{P_t}{P_2} = \frac{P_o}{P_2} \cdot \frac{P_t}{P_o} \quad , \tag{C-4}$$

and then express $P_t/P_2$ in terms of $M_2$ by using Eqs. (C-1) through (C-3). Substituting these expressions in Eq. (C-4), we obtain

$$\frac{P_t}{P_2} = \left[ \frac{(\frac{\gamma + 1}{2} M_2^2)^\gamma}{\frac{2\gamma}{\gamma + 1} M_2^2 - \frac{\gamma - 1}{\gamma + 1}} \right]^{1/\gamma - 1} \quad . \tag{C-5}$$

This is the Rayleigh-Pitot formula that is valid for Mach numbers greater than one.

For subsonic flow about a probe oriented as shown in Fig. 10, no standing shock wave is formed. Therefore, Eq. (C-5) is not applicable. In this case the ordinary isentropic relation,

$$\frac{P_t}{P_2} = (1 + \frac{\gamma - 1}{2} M_2^2)^{\gamma/(\gamma-1)} \quad , \tag{C-6}$$

is used to relate the static pressure, stagnation pressure and Mach number. If one can measure any two of the parameters, the other one can be predicted.

By locating a pressure measuring device such as the sensitive head of a piezoelectric pressure transducer at the stagnation point, one can measure the stagnation pressure and then use the above equation to calculate the flow velocity if the free-stream pressure $P_2$ is available. If the flow being studied is that behind a normal shock wave, both the free-stream pressure and velocity can be predicted from a measurement of the shock-wave velocity. Under circumstances such as these, the stagnation pressure measurements can be used for calibrating pressure probes and for studying flow phenomena in the noncontinuum regime.

## ACKNOWLEDGMENTS

We extend our thanks to Dr. R. Taylor of the AVCO-Everett Research Laboratory and to Drs. W. H. Parkinson and E. M. Reeves of the Harvard College Observatory for their kindness in permitting us to use their shock-tube facilities. Our many discussions with Prof. Eugene Covert, Aerophysics Laboratory, M. I. T. have guided our thoughts and sharpened our understanding of the fluid mechanics aspects of this investigation. The cooperation of Messrs. W. Worthington, C. Kilcline and J. Cataldo of Lincoln Laboratory is gratefully acknowledged.

## REFERENCES

1. W. M. Kornegay, "Production and Propagation of Spherical Shock Waves at Low Ambient Pressures," Technical Report 375, Lincoln Laboratory, M. I. T. (26 January 1965) (in press).
2. J. D. Fridman, W. M. Kornegay and W. C. Worthington, "The Propagation of Spherical Shock Waves into Ionized Media" (in preparation).
3. F. Massa, "Piezoelectric Sound Pressure Microphone," U. S. Patent No. 2,472,714 (1949).
4. R. E. Duff, Phys. Fluids 2, 207 (1959).
5. A. Roshko, Phys. Fluids 3, 835 (1960).
6. W. J. Hooker, Phys. Fluids 4, 1451 (1961).
7. G. Rudinger, Phys. Fluids 4, 1463 (1961).
8. H. E. Petshek and S. Byron, Ann. Phys. 1, 270 (1957).
9. K. E. Harwell and R. G. Jahn, Phys. Fluids 7, 214 (1964).
10. I. Amdur and E. A. Mason, Phys. Fluids 1, 370 (1958).
11. F. S. Sherman, "New Experiments on Impact Pressure Interpretation in Supersonic and Subsonic Rarefied Air Streams," Technical Note 2995, National Advisory Committee for Aeronautics (September 1953).
12. C. G. Hylkema and R. B. Bowesox, "Experimental and Mathematical Techniques for Determining the Dynamic Response of Pressure Gages," Memo. No. 20-68, Jet Propulsion Laboratory, C. I. T. (1953).
13. R. T. Eckenrode and H. A. Kirshner, Rev. Sci. Instr. 25, 33 (1954).
14. K. R. Enkenhus, "Pressure Probes at Very Low Density," UTIA Report No. 43, Institute of Aerophysics, University of Toronto (January 1957).
15. S. I. Kosterin, et al., Inzh.-Fiz. Zh. 5, No. 12, 16 (1962). Translated as AR Memo 698, Aerophysics Laboratory, M. I. T. (April 1963).

16. W. R. Schowalter and G. E. Blaker, Trans. ASME 28E, 136 (March 1961).

17. J. L. Potter and A. B. Bailey, "Pressures in the Stagnation Regions of Blunt Bodies in the Viscous-Layer to Merged-Layer Regimes of Rarefied Flow," Technical Documentary Report No. AEDC-TDR-63-168, Arnold Engineering Development Center, AFSC, Tennessee (1963).

18. R. F. Probstein and N. H. Kemp, "Viscous Aerodynamic Characteristics in Hypersonic Rarefied Gas Flow," J. Aero/Space Sci. 27, 174 (1960).

19. J. H. Gerrard, "Piezoelectric Pressure Gauges for Use in a Shock Tube," Acustica 9, 17 (1959).

20. W. G. Cady, Piezoelectricity (McGraw-Hill, New York, 1960).

21. R. K. Lobb, "On the Length of a Shock Tube," UTIA Report No. 4, Institute of Aerophysics, University of Toronto (July 1950).

22. H. Liepmann and A. Roshko, Elements of Gas Dynamics (Wiley, New York, 1957).

23. I. Glass, "Theory and Performance of Simple Shock Tubes," UTIA Review No. 12, Part I, Institute of Aerophysics, University of Toronto (May 1958).

24. H. A. Bethe and E. Teller, "Deviations from Thermal Equilibrium in Shock Waves," Report No. X-117, Ballistic Research Laboratories, Aberdeen Proving Ground, Maryland (1945).

25. J. G. Hall, "Shock Tubes: Production of Strong Shock Waves, Shock Tube Application, Design and Instrumentation," UTIA Review No. 12, Part II, Institute of Aerophysics, University of Toronto (May 1958).

26. A. B. Cambel and B. H. Jennings, Gas Dynamics (McGraw-Hill, New York, 1958).

27. F. W. Geiger, C. W. Mautz and R. N. Hollyer, "The Shock Tube as an Instrument for the Investigation of Transonic and Supersonic Flow Patterns," Engineering Research Institute Report, University of Michigan (June 1949).

## DOCUMENT CONTROL DATA – R&D

*(Security classification of title, body of abstract and indexing annotation must be entered when the overall report is classified)*

1. ORIGINATING ACTIVITY *(Corporate author)*
Lincoln Laboratory, M. I. T.

2a. REPORT SECURITY CLASSIFICATION
Unclassified

2b. GROUP

3. REPORT TITLE
Calibration of a Pressure Sensor for Measurements in Continuum and Rarefied Gas Flows

4. DESCRIPTIVE NOTES *(Type of report and inclusive dates)*
Technical Report

5. AUTHOR(S) *(Last name, first name, initial)*
Kornegay, W. M. and Fridman, J. D.

6. REPORT DATE
8 February 1965

7a. TOTAL NO. OF PAGES
28

7b. NO. OF REFS
27

8a. CONTRACT OR GRANT NO.
AF 19(628)-500

b. PROJECT NO.
ARPA Order 600

c.

d.

9a. ORIGINATOR'S REPORT NUMBER(S)
Technical Report 379

9b. OTHER REPORT NO(S) *(Any other numbers that may be assigned this report)*
ESD-TDR-65-43

10. AVAILABILITY/LIMITATION NOTICES

11. SUPPLEMENTARY NOTES

12. SPONSORING MILITARY ACTIVITY
Advanced Research Projects Agency, Department of Defense

13. ABSTRACT

The free-stream flow behind shock waves produced in the laboratory has been used to obtain a dynamic calibration of a highly sensitive piezoelectric pressure sensor under a wide variety of conditions. Experimental results on the influence of rarefied gas flow on the value of stagnation pressure measured with the sensor are described. This report covers the continuum, slip and transition flow regimes. Design characteristics of the pressure sensor are presented and experimental results are discussed in view of the impact pressure measurements of other authors.

14. KEY WORDS

pressure sensor
gas flow
piezoelectric
shock tubes
spherical shock waves
low-pressure effects
Mach number
Rayleigh theory

Printed by
United States Air Force
L. G. Hanscom Field
Bedford, Massachusetts